CHAPTER IV
RESULTS AND DISCUSSION

4.1 Synthesis of the Nano-crystalline KL Zeolite (NCL)

The nano-crystalline KL (NCL) was synthesized by microwave-hydrothermal treatment and characterized by XRD, TEM and DLS. The XRD pattern of the NCL is compared to that of the commercial KL zeolite (COM) as shown in Figure 4.1. The XRD patterns indicate that both samples are highly crystalline LTL-type material, without any trace of other crystalline phases or amorphous materials. The NCL exhibits very broad XRD peaks, indicating the presence of very small crystals (Vaughan, 1994).

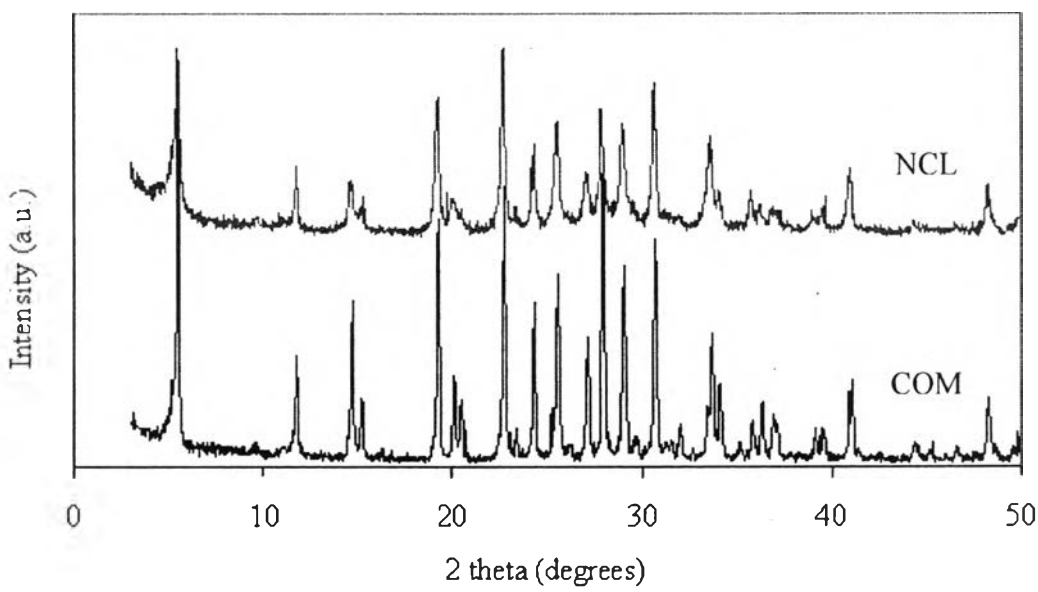

Figure 4.1 XRD patterns of nano-crystalline KL zeolite (NCL) and commercial KL zeolite (COM).

In good agreement with XRD result, the TEM image depicted in Figure 4.2 indicates that the zeolite crystals have dimension of approximately 20 nm in the channel direction; however, these crystals tend to agglomerate into larger particle

having approximately 0.14 μm in size determined by the DLS method. However, the particle size measured by DLS showed that the size of NCL is much smaller than that of COM as illustrated in Table 4.1

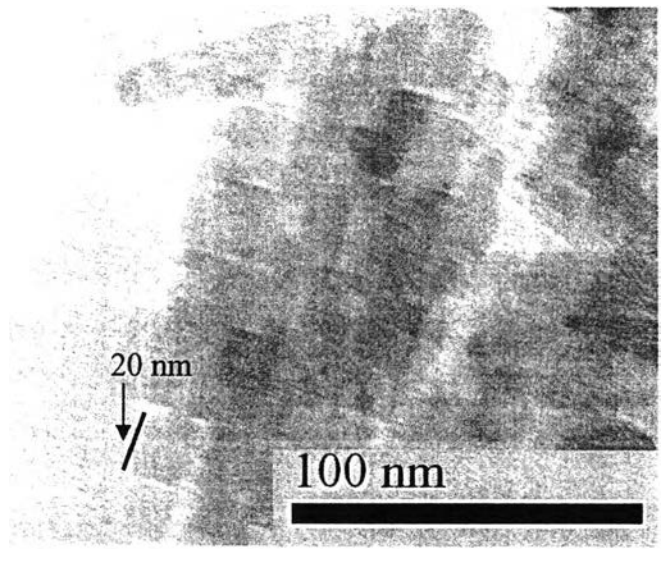

Figure 4.2 TEM image of synthesized nano-crystalline KL zeolite (NCL) at 175°C for 8 h.

Table 4.1 The comparison between the particle sizes of COM and NCL measured by DLS method

KL zeolites	Particle size (μm)
COM	0.41
NCL	0.14

FTIR is another technique employed to verify the crystallinity of the synthesized KL zeolites. Spectra of the NCL and COM are compared as shown in Figure 4.3. The results show that both spectra of KL zeolites are similar. As previous report (Joshi *et al.*, 1990), an absorption band centered around 600 cm^{-1} is the characteristic of crystalline KL zeolites, such results are in good agreement with those obtained by XRD measurement.

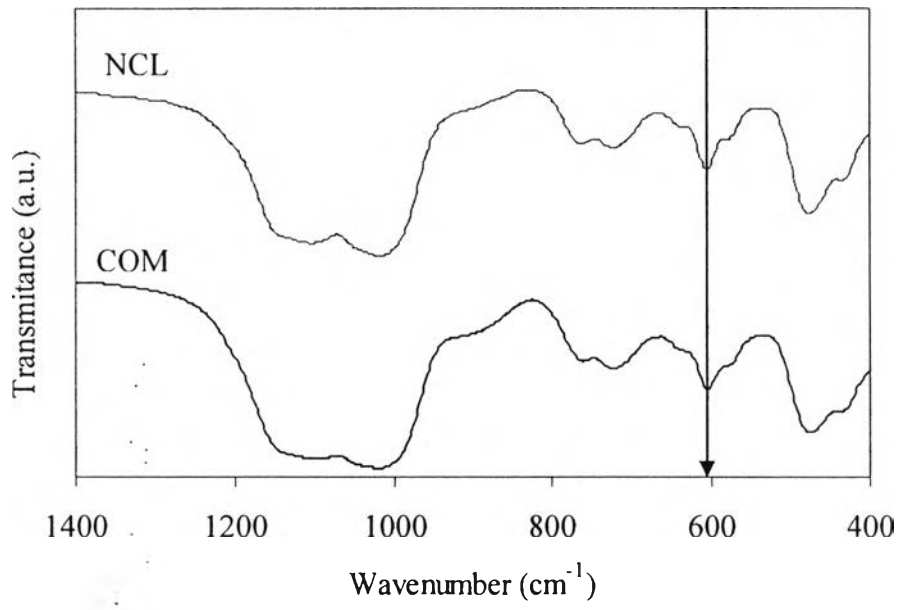

Figure 4.3 FTIR spectra of nano-crystalline KL zeolite (NCL) obtained at aging time of 17 h and crystallization time of 8 h synthesized by microwave hydrothermal treatment compared to that of commercial KL zeolite (COM).

4.2 Characterization of the Fresh Catalysts

Table 3.1 shows a list of the different bimetallic Pt/Sn molar ratios for the catalysts supported on NCL and COM prepared by vapor phase co-impregnation method. To determine the behavior of Sn, the bimetallic Pt-Sn/KL catalysts were characterized by TEM and TPR. TEM images of metal size distribution of mono- and bi- metallic Pt-Sn/KL catalysts are illustrated in Figure 4.4. The results show that the addition of Sn decreases the particle size of metal compare with the catalyst without employing Sn. The metal clusters are well dispersed on 1Pt1Sn/COM compared with 1Pt1Sn/NCL and 1Pt0.6Sn/NCL.

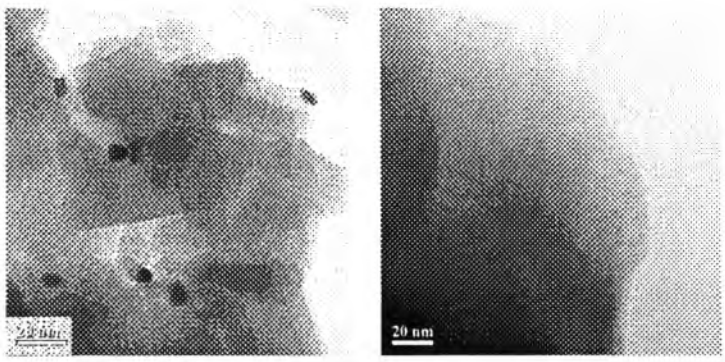

1Pt/COM 1Pt1Sn/COM

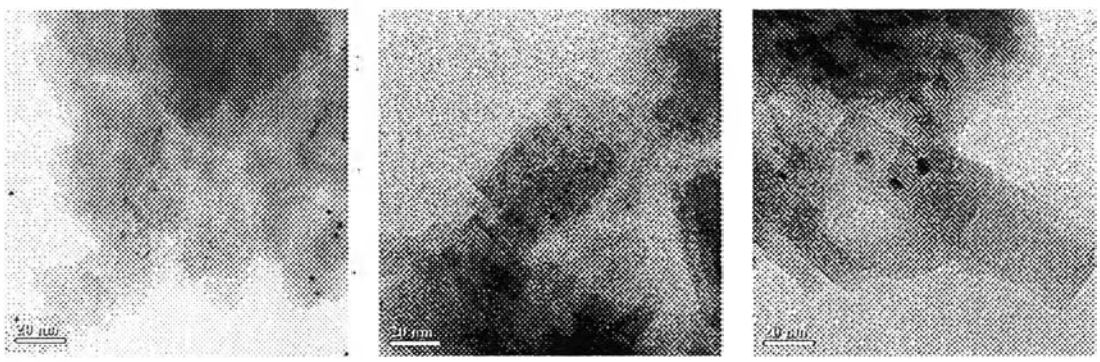

1Pt/NCL 1Pt0.6Sn/NCL 1Pt1Sn/NCL

Figure 4.4 TEM images of metal size distribution obtained by TEM of the mono- and bi- metallic Pt-Sn/KL catalysts.

Table 4.2 Analysis of fresh and spent catalysts

Catalyst	Pt (wt%)	Sn (wt%)	H/Pt ratio after reduction at 500°C	Coke deposited after reaction 550 min time on stream (wt%)
1Pt/COM	1	1	1.70	2.78
1Pt/NCL	1	0	0.43	3.30
1Pt1Sn/COM	1	1	0.15	2.58
1Pt0.6Sn/NCL	1	0.6	0.25	3.21
1Pt1Sn/NCL	1	1	0.10	2.60

TPR experiment was carried out to investigate the reducibility of samples. Figure 4.5 shows the TPR profiles of the mono- and bi- metallic Pt-Sn supported on NCL and COM. For the monometallic 1Pt catalyst, a broad reduction peak centered at ca.175°C represents to the reduction of Pt (IV) to Pt° (Ostgard *et al.*, 1992; Zheng *et al.*, 1996; and Rodriguez *et al.*, 2005). This profile also shows some H_2 consumption at about 400°C. However, this is not due to the reduction of Pt species, but rather to the removal of impregnation precursor which was not totally eliminated during the initial calcination step (Stagg *et al.*, 1997). In contrast, the TPR of 1Sn shows one broad reduction peak starting at 300°C with the maximum around 600°C (Trakarnroek *et al.*, 2007). When the profiles of the both monometallic 1Pt and 1Sn catalysts were combined, it was not match with any profile of the bimetallic Pt-Sn/KL catalysts. The TPR profiles of the bimetallic Pt-Sn catalyst supported on COM and NCL can be deconvoluted into three main peaks which correspond to Pt (IV) to Pt° (Pt rich phase), PtSn alloy phase, and Sn rich phase as demonstrated in Table 4.3. From these data, 1Pt1Sn/COM exhibits higher fraction of PtSn alloy phase than other two bimetallic catalysts.

The results of the hydrogen chemisorptions are reported in Table 4.2. The monometallic 1Pt catalyst shows a high H/Pt ratio compared to the bimetallic Pt-Sn catalysts. Therefore, addition of Sn caused a strong decrease in the H/Pt ratio. It was found that the decreasing of the H/Pt ratio of the bimetallic Pt-Sn catalysts depends on the fraction of alloy formation. This demonstrated that the addition of Sn obviously depressed the availability of surface Pt atoms due to the PtSn alloy formation.

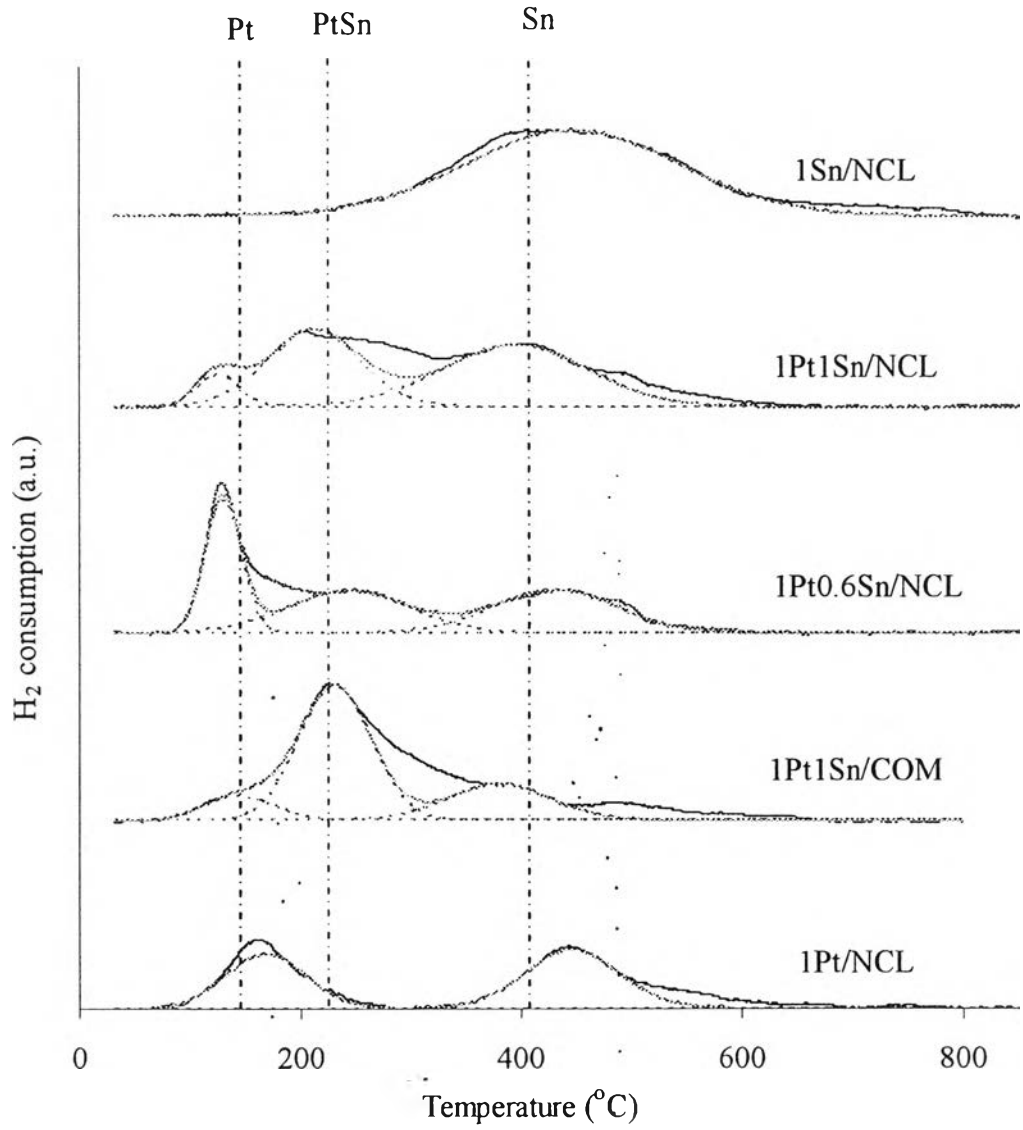

Figure 4.5 TPR profiles of the different Pt/Sn ratio of mono- and bi- metallic Pt-Sn catalysts prepared by vapor phase co-impregnation.

Table 4.3 Deconvolution of TPR profiles of bimetallic Pt-Sn/KL catalysts

Catalysts	Area of each TPR peak (%)		
	100-250°C Pt-rich phase	180-300°C Pt-Sn alloy phase	300-600°C Sn-rich phase
1Pt1Sn/COM	11.12	62.29	26.59
1Pt0.6Sn/NCL	31.13	33.80	35.07
1Pt1Sn/NCL	7.48	40.79	51.73

X-ray photoelectron spectra of the Pt4f level were recorded in order to obtain information about the oxidation states of the metal phased on the surface. The peak positions have been corrected for sample charging by using the Si2p peak as a standard at 102.0 eV. Figure 4.6 shows the Pt4f spectra of 1Pt/COM and 1Pt1Sn/COM after reduction with hydrogen for 1 h at 500°C. The relative intensities of different species from the curve-fitted XP spectra and their binding energy (B.E.) are reported in Table 4.4. The Pt4f photoelectron line mainly consists of two doublets of increasing binding energies (B.E.), assigned to Pt metal and PtO. The presence of metallic Pt(0) of 1Pt/COM, characterized by the $4f_{7/2}$ and $4f_{5/2}$ peak doublet with the B.E at 71.05 and 74.45 eV, respectively (Hoang *et al.*, 2007). The presence of the above reported oxidized platinum species is quite evident at higher B.E. (Neri *et al.*, 2007), i.e. PtO at about 71.57 and 74.87. After addition of Sn, when PtSn alloys were formed, an electron transfer from Sn to Pt can occur. Consequently, $Pt4f_{7/2}$ components which gain electronic density from Sn are shift to lower B.E. as shown in Figure 4.6 and Table 4.4. Most recently, It was found that observed a similar shift towards lower B.E. for the $Pt4f_{7/2}$ signal of Pt-Sn/SiO_2 catalysts prepared by surface organometallic reactions versus Pt/SiO_2. This effect was attributed to an electron transfer from Pt4f level to the Pt–Sn bond. The combined TPR and XPS data could be explained by assuming that platinum is alloyed with Sn or even electronically modified by the Sn presence. In this work, it was only found that PtSn alloy formation causes the decreasing of metal size compared to no alloy phase formation.

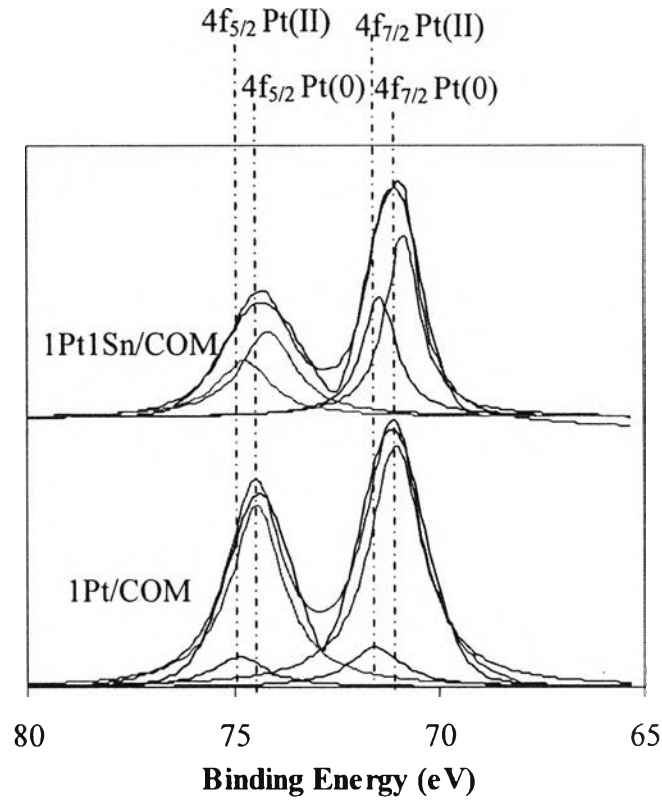

Figure 4.6 Pt4f XPS spectra of 1Pt/COM and 1Pt1Sn/COM after hydrogen treatment for 1 h at 500°C (reduced).

Table 4.4 Binding energies and relative intensities of different species from curve-fitted XPS spectra of various catalysts

Sample	Species	Binding Energy (eV)		Relative Peak Area (%)
1Pt/COM		Pt $4f_{7/2}$	Pt $4f_{5/2}$	
	Pt(0)	71.05	74.45	85.82
	Pt(II)	71.57	74.87	14.18
1Pt1Sn/COM		Pt $4f_{7/2}$	Pt $4f_{5/2}$	
	Pt(0)	70.87	74.17	60.44
	Pt(II)	71.44	74.74	39.56

4.3 Catalytic Activity Testing: *n*-Octane Aromatization

As reported in the previous work, Pt supported on nanocluster KL zeolite as the catalyst for *n*-octane aromatization exhibited good selectivity to C8-aromatic product compared to Pt supported on longer channel length KL zeolite because the diffusion limitations of C8-aromatics were improved, leading to the inhibition of the hydrogenolysis reaction occurring inside the pore. Furthermore, it was found that the addition of Sn on the Pt/KL catalyst showed the better stability and selectivity to C8-aromatics than without addition of Sn. Therefore, PtSn supported on nanocluster KL zeolite might be the good catalyst used for improvement of the activity and C8-aromatics selectivity for *n*-octane aromatization. The 1Pt/COM, 1Pt/NCL, 1Pt1Sn/COM, 1Pt1Sn/NCL, and 1Pt0.6Sn/NCL catalysts were tested for *n*-octane aromatization at 500°C and 1 atm. The variation of *n*-octane conversion with time on stream for the monometallic catalyst is illustrated in Figure 4.7 (a). 1Pt/NCL exhibits lower activity and stability than 1Pt/COM. Even though 1Pt/COM and 1Pt/NCL give high n-octane conversion at first few hours on stream, the activity exhibits a rapid deactivation due to coke plugging inside the pores because of the restricted diffusion out of the pore of C8-aromatics products (EB and OX) (Jongpatiwut *et al.*, 2005). In term of product selectivity, although 1Pt/COM gives higher total aromatic selectivity than 1Pt/NCL, it gives higher selectivity to C8-aromatics as shown in Figure 4.7 (b) and (c). It means that the longer channel length KL zeolite which is COM increases the residence time of the C8-aromatics products inside the zeolite. Consequently, there is high probability to undergo secondary hydrogenolysis reaction into benzene and toluene with small amount of EB and OX as shown in Table 4.5.

Table 4.5 *n*-Octane conversion and product distribution over 1Pt/COM, 1Pt/NCL, 1Pt1Sn/COM, 1Pt1Sn/NCL, and 1Pt0.6Sn/NCL catalysts tested for *n*-octane aromatization after 550 min time on stream (Reaction condition; temperature = 500°C, pressure = 1 atm, WHSV = 5 h^{-1}, H_2:HC = 6:1)

Properties	1Pt/COM*	1Pt/NCL	1Pt1Sn/COM	1Pt0.6Sn/NCL	1Pt1Sn/NCL
Conversion (%)	23.28	13.94	57.46	41.43	32.77
Product distribution (%)					
C1-C5	19.72	20.02	3.94	4.78	4.45
Total enes (C6-C8enes)	12.40	29.56	24.96	30.37	34.73
Total aromatics	67.88	50.42	71.10	64.85	60.82
Total aromatics (%)					
Benzene	19.05	4.02	0.48	6.41	3.23
Toluene	27.59	19.87	0.59	10.09	15.63
C8-aromatics (%)	21.24	26.53	70.03	48.35	41.96
Ethylbenzene (EB)	13.95	15.27	26.91	21.85	19.62
m-, p-Xylene	1.82	2.34	1.91	0	1.78
o-Xylene (OX)	5.47	8.92	41.21	26.50	20.56
EB/OX ratio	2.55	1.71	0.65	0.82	0.95
Hydrogenolysis products	66.36	43.91	5.01	21.28	23.31

*The data were obtained from previous work: S.Trakarnroek et al.,

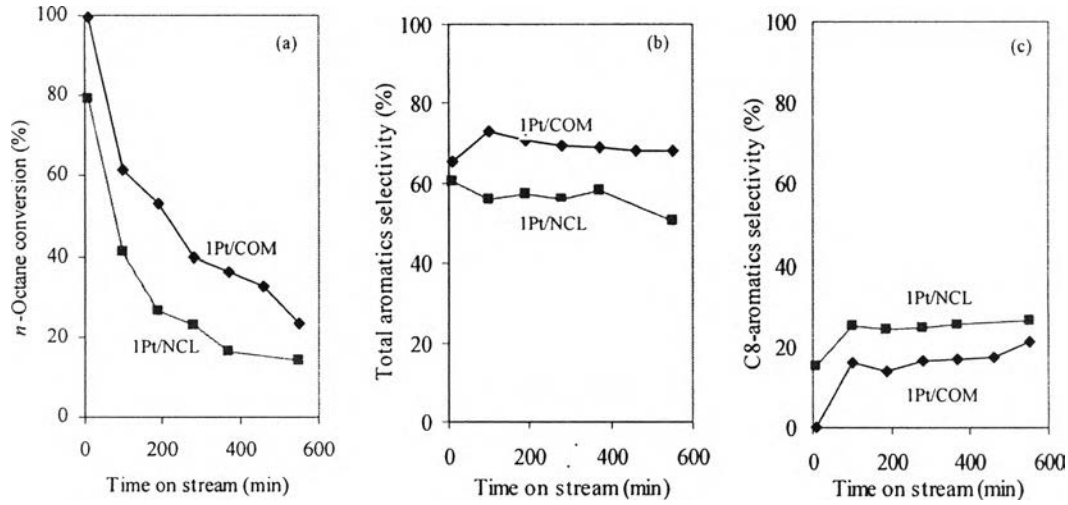

Figure 4.7 The variations of (a) *n*-octane conversion (b) total aromatics selectivity and (c) C8-aromatics selectivity with time on stream (Catalysts: 1Pt/COM and 1Pt/NCL. Reaction condition; temperature = 500°C, pressure = 1 atm, WHSV = 5 h^{-1}, H_2:HC = 6:1).

In a previous study, it was found that the addition of Sn improved the stability of the Pt/KL catalyst by inhibiting the adsorption of dehydrogenated species which was the intermediate of coke. Sn addition breaks the Pt ensemble into the small metal clusters. Consequently, the coke and hydrogenolysis reaction which favor to occur on large metal ensemble is inhibited (Passos *et al.*,1998). Addition of Sn on the Pt/KL supported on both COM and NCL enhances activity and C8-aromatics selectivity of *n*-octane aromatization as shown in Figure 4.8. Using COM zeolite as a support gives higher activity and C8-aromatics selectivity than using NCL zeolite. This could be due to 1Pt1Sn/COM has high amount of PtSn alloy even though COM zeolite has longer channel length. This indicates that the presence of PtSn alloy plays an important role in the catalytic activity for *n*-octane aromatization than the channel length zeolite. In case of 1Pt1Sn/COM and 1Pt0.6Sn/NCL, the activity and C8-aromatics selectivity corresponded with the fraction of PtSn alloy formation as ascribed in Figure 4.5 and Table 4.3. For the TPR analysis of 1Pt0.6Sn/NCL and 1Pt1Sn/NCL, it was found that the higher the amount of Sn, the lower the amount of Pt rich phase, Consequently, there is higher fraction of PtSn

alloy phase observed as increasing the amount of Sn. However, the activity of the bimetallic Pt-Sn/KL is decreased when excess amount of Sn was added (Trakarnroek *et al.*, 2007). As shown in Figure 4.8, Even though 1Pt1Sn/NCL has higher fraction of alloy formation than 1Pt0.6Sn/NCL, its activity and stability are less than those of 1Pt0.6Sn/NCL. This is postulated that an excess amount of Sn might cover the active sites and alloy phase; resulting in decreasing the activity and stability. Somehow, it was observed that even though the stability of the 1Pt0.6Sn/NCL, was improved, the amount of coke deposits is similar to 1Pt/NCL, except for 1Pt1Sn/NCL and 1Pt1Sn/COM as reported in Table 4.2. The predominant aromatics product obtained from the bimetallic catalysts, 1Pt1Sn/COM, 1Pt1Sn/NCL and 1Pt0.6Sn/NCL, are C8-aromatics (EB and OX) with small quantities of benzene and toluene. However, less selectivity to total aromatics and C8-aromatics was observed when excess amount of tin was added as demonstrated in Table 4.5.

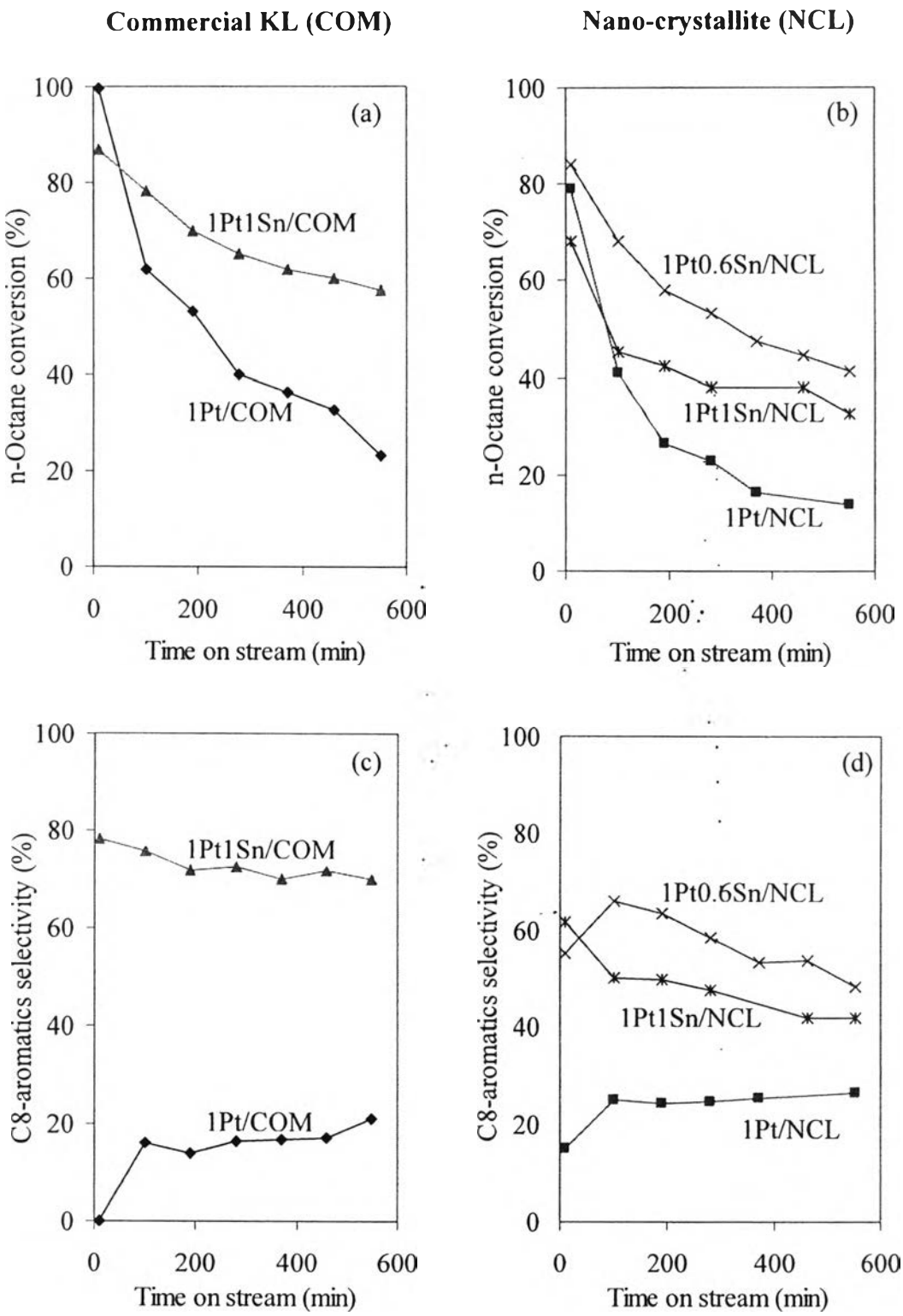

Figure 4.8 The variations of *n*-octane conversion and C8-aromatics selectivity on mono- and bi- metallic Pt-Sn supported on (a), (c) COM and (b), (d) NCL with time on stream (Reaction condition; temperature = 500°C, pressure = 1 atm, WHSV = 5 h^{-1}, H_2:HC = 6:1)

Moreover, combination results from XPS and TPR, it was believed that Sn decreased the hydrogenolysis reaction by electronic effect since some electrons of Sn were transferred to Pt when PtSn alloy was formed. Consequently, C-C bond hydrogenolysis does not occur because the hydrocarbon cannot be strongly adsorbed on the catalyst surface. Not only was the hydrogenolysis reaction decreased by the addition of Sn, but the formation of OX molecules was also enhanced as shown in Table 4.5. Westfall *et al.* (1976) and Lee *et al.* (1993) informed that the molar ratio of EB/OX may be an indirect index, indicating that electron density of Pt by the addition of Sn. Dehydrocyclization of *n*-octane produced EB and OX by a mechanism that involves the direct formation of a six-membered carbon ring (Davis *et al.*, 1969). The bond strength of primary hydrogen in $-CH_3$ is only greater than that of secondary hydrogen in $-CH_2$. Therefore, it was expected that the six-membered ring intermediate would lead to an almost equal amount of EB and OX (Meriaudeau *et al.*, 1997). However, Sn would alter the ability of Pt to rupture the C-H bond and favor the rupture of the weaker C-H bond of the secondary hydrogen of the $-CH_2$ groups over those of the primary hydrogen of the $-CH_3$ groups. Therefore, the EB/OX ratio was decreased when Sn was employed (Trakarnroek *et al.*, 2007). From Table 4.5, it was found that the EB/OX ratio of 1Pt/COM and 1Pt/NCL are significantly high as a result of no electrons being transferred from Sn to Pt atoms. The bimetallic catalyst of 1Pt1Sn/COM, 1Pt1Sn/NCL and 1Pt0.6Sn/NCL exhibit the EB/OX ratio less than unity. 1Pt1Sn/COM yielded a favorable EB/OX ratio of 0.65 while 1Pt1Sn/NCL, and 1Pt0.6Sn/NCL yielded less than favorable results 0.95, and 0.82, respectively. On the other hand, the 1Pt/COM and 1Pt/NCL are greater than unity. The reason 1Pt/COM and 1Pt/NCL are greater than one because the critical size of the OX molecule is larger than that of EB which means the speed of transport through the pores is slower for OX than for EB. Therefore, OX is much easier to convert to smaller molecules such as benzene, toluene and methane by secondary hydrogenolysis. Both geometric and electronic effects are important factors on the catalytic activity in the *n*-octane aromatization for inhibition of hydrogenolysis reaction and enhancement in C8-aromatics.

4.4 Regeneration in Air of Deactivated 1Pt1Sn/COM Catalysts

The condition for the regeneration in air of 1Pt1Sn/COM catalysts was investigated in terms of catalytic activity such as conversion and selectivity. The catalysts were characterized by means of TPR, XPS and TPO providing the reducibility of samples, Pt-Sn interaction and amount of carbon deposits on catalyst, respectively.

The activity of catalyst was measured as a function of *n*-octane conversion versus time on stream, C8-aromatics selectivity, total aromatics selectivity and EB/OX ratio after 370 min on stream after regeneration. The results and discussion of the study of the effect of experimental parameters toward the regeneration are divided into 3 parts. (I) Effect of regeneration temperature (II) Effect of regeneration time (III) Effect of regeneration air flow rate.

4.4.1 Effect of Regeneration Temperature

In this part, catalytic activity measurement and catalyst characterization were discussed.

4.4.1.1 Catalytic Activity Measurement

Figure 4.9 shows the variation of *n*-octane conversion at 500°C without regeneration in air.

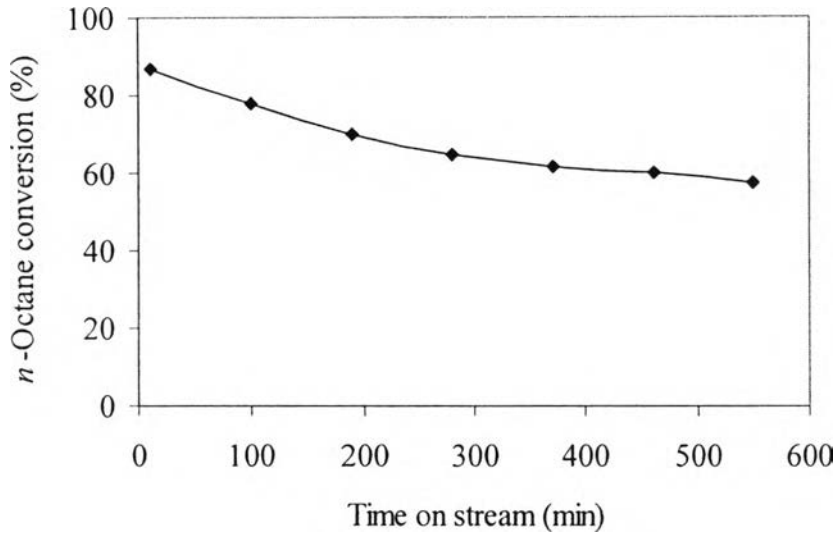

Figure 4.9 The variation of *n*-octane conversion at 500°C without regeneration in air.

Although addition of Sn enhances the catalytic performance of *n*-octane aromatization in term of conversion and selectivity, 1Pt1Sn/COM will be deactivated by coke plugging inside the pores after 550 min on stream (Trakarnroek *et al.*, 2007). Consequently, it was also found that deactivated Pt/KL catalysts for *n*-octane aromatization can be regained by oxidizing the coke deposits with air. The initial activity and the deactivated pattern were almost identical to that of the fresh catalyst after the *in situ* regeneration (Jongpatiwut *et al.*, 2003). Therefore, the spent 1Pt1Sn/COM can be regenerated with air as an oxidant agent in this work.

Figure 4.10 to Figure 4.13 show the *n*-octane conversion, C8-aromatics selectivity, total aromatics selectivity and EB/OX ratio after 370 min on stream of regenerated catalyst with air at various regeneration temperatures (300-500°C), respectively. The most suitable regeneration conditions must be able to recover catalytic performance and structural properties of catalysts as close as possible of the fresh catalyst. Moreover, EB/OX ratio was considered to indicate diffusional effects that limit the production of C8-aromatics which are desired product for *n*-octane aromatization (Jongpatiwut *et al.*, 2003). The lower the EB/OX ratio, the lower the diffusional effects.

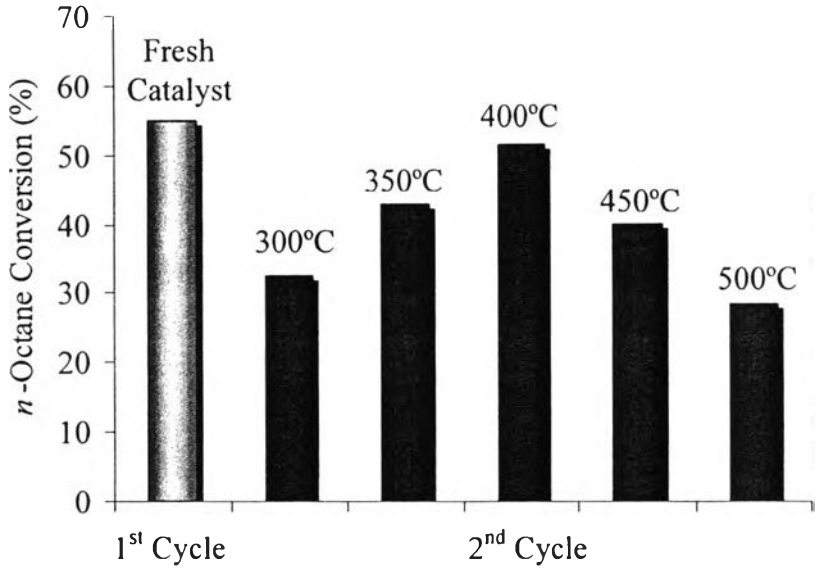

Figure 4.10 The *n*-octane conversion after 370 min on stream of regenerated catalysts at various regeneration temperatures (300-500°C).

Initially, as presented in Figure 4.10, it can observe a progressive recovery of the conversion of *n*-octane as the regeneration temperature increase from 300 to 400 °C (Figure 4.10). Although the activity increases with temperature, the activity still performs low conversion of *n*-octane aromatization due to residual high carbon content as illustrate in Table 4.7. The regeneration temperature at 400°C performs the particular highest conversion of *n*-octane aromatization because the conversion of the regenerated 1Pt1Sn/COM catalyst can be regained closely to the original of the fresh 1Pt1Sn/COM. It might be due to the effect of coke reduction. On the other hand, the regeneration temperature above 400°C shows low conversion of *n*-octane aromatization since the regeneration at high temperature might be disrupted some PtSn alloys as demonstrated in TPR profiles (Figure 4.14).

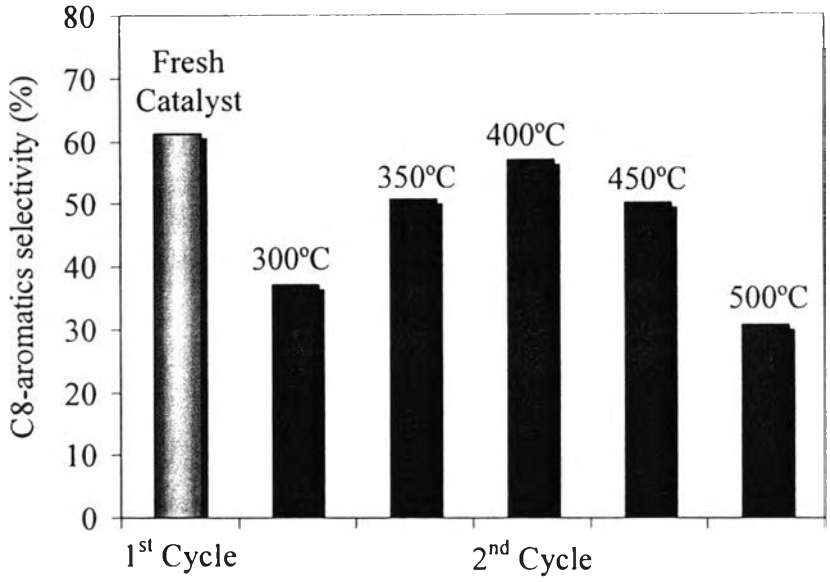

Figure 4.11 The C8-aromatics selectivity after 370 min on stream of regenerated catalysts at various regeneration temperatures (300-500°C).

In a range of 300-400°C, C8-aromatics selectivity increases with temperature at regeneration temperature. Regeneration temperature at 400°C is greatly high compared with that obtained from the other regeneration conditions as shown in Figure 4.11. The regeneration temperature above 400°C displays the low C8-aromatics selectivity. It could be due to the high regeneration temperature which destroys the PtSn alloys which cause the high selectivity of C8-aromatics (Trakarn-roek *et al.*, 2007).

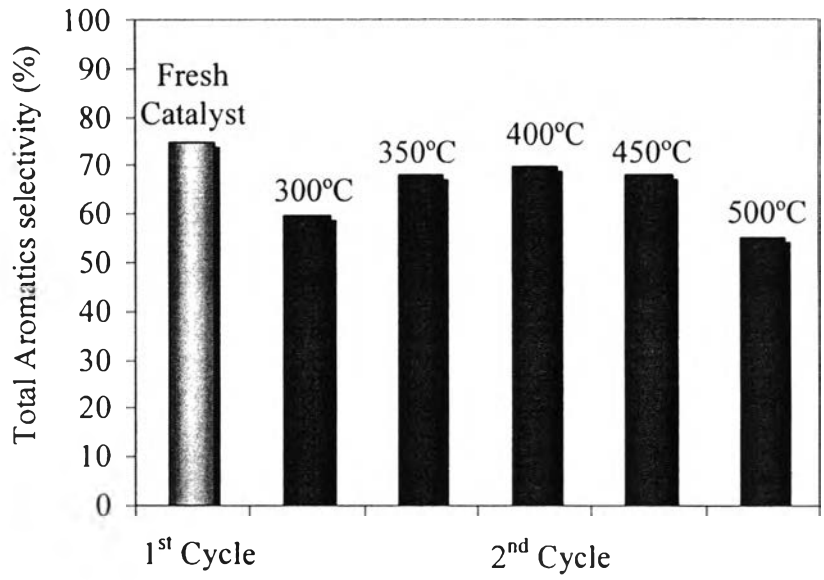

Figure 4.12 The total aromatics selectivity after 370 min on stream of regenerated catalysts at various regeneration temperatures (300-500°C).

Figure 4.12 presents the total aromatics selectivity of the regeneration temperature in range 350-450°C is slightly different but the regeneration temperature at 400°C obtained the closest total aromatics selectivity to the fresh 1Pt1Sn/COM. The total aromatics selectivity at 300°C of regeneration temperature performs the low selectivity compare to the other conditions. It might be due to residual high carbon content that still covers some parts of the catalyst.

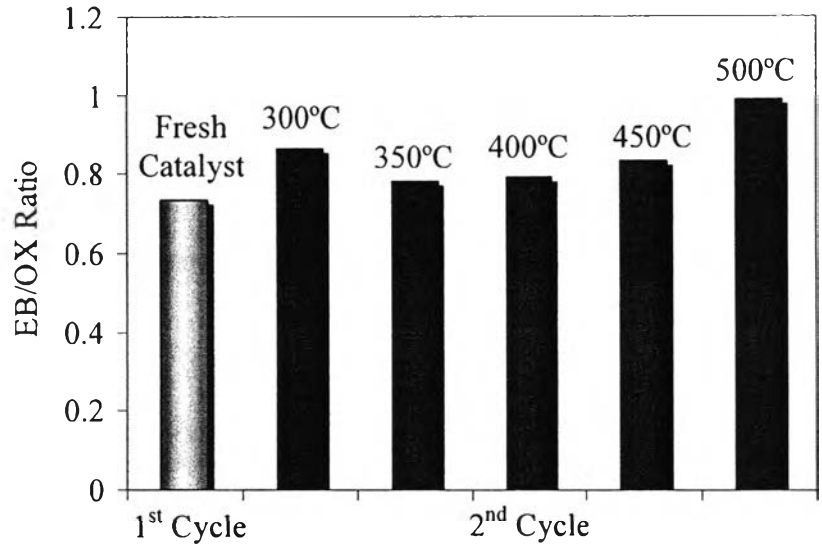

Figure 4.13 The EB/OX ratio after 370 min on stream of regenerated catalysts at various regeneration temperatures (300-500°C).

Interestingly, the EB/OX ratios at various regeneration temperatures are slightly different, as illustrated in Figure 4.13. The EB/OX ratio on the lower regeneration temperature seems to increase slightly. This slight difference could be due to an inhibition of the OX mobility inside the channels of the zeolite caused by the presence of the fraction of carbon residues in the regenerated catalysts. This restrictive movement results in a longer residence time of OX than EB inside the zeolite channels (Jongpatiwut *et al.*, 2003).

Therefore, regeneration at 400°C seems to be the best condition temperature, since the catalytic activity and selectivity are very close to the data that obtained from the fresh sample.

4.4.1.2 Characterization of Catalysts

Fresh, spent and regenerated catalysts were characterized by means of TPR, XPS and TPO.

(I) Temperature Programmed Reduction (TPR)

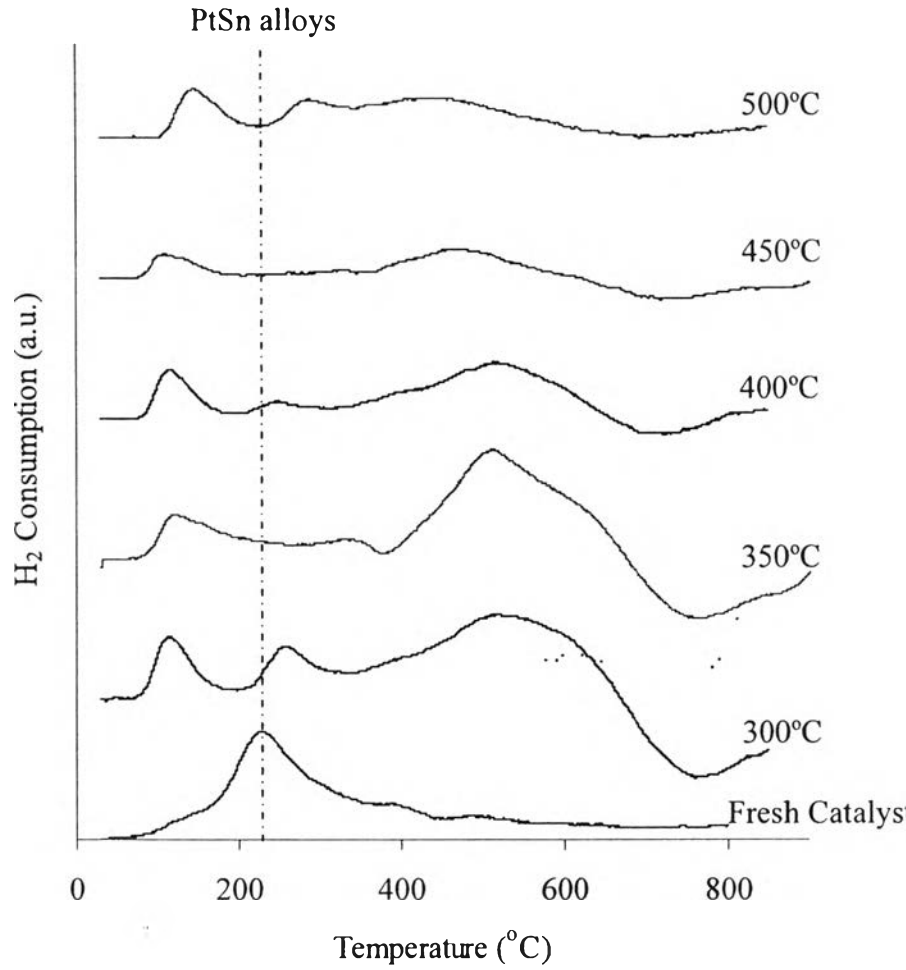

Figure 4.14 TPR profiles of regenerated catalysts at various regeneration temperatures (300-500°C).

To investigate the reducibility of sample, a TPR study was carried out. Figure 4.14 displays the TPR profile of the regenerated catalysts and shows interesting changes with increasing temperature of regeneration, as compared to the fresh Pt-Sn/COM. In our previous study, the 1Pt/COM was found to display a main reduction peak centered at 175°C, which corresponds to the reduction of Pt(IV) to Pt(0). The TPR profile of 1Sn/COM showed one broad reduction peak starting at 300°C with the maximum around 420°C. When the profiles of the two monometallic

catalysts 1Pt and 1Sn, the profile of Pt-Sn/COM shows only one sharp peak at 230°C as shown in Figure 4.14.

From the TPR profiles, it is clearly seen that part of PtSn alloys has been broken after the regeneration especially at high temperature. At regeneration of 300°C and 350°C, the TPR profile is distorted. Although high amount of PtSn alloys is observed on two regenerated catalysts, the catalytic performance is still low, probably because the high residual coke covering the PtSn alloys. In addition, a desorption peak appears at high temperature (above 400°C). This desorption phenomena corresponds to cracking/desorption reactions on residual coke, together with some carbon gasification which are known to be catalyzed by noble metals under H_2 atmosphere (Marécot *et al.*, 1990). In a separate experiment, the desorption products formed during TPR experiments were monitored by on-line gas chromatography (Afonso *et al.*, 1995). Hydrocarbons (aliphatic/aromatic), together with small amounts of methane, were detected. Interestingly, when the regeneration temperature was increased, the desorption peak was also decreased because high amount of coke was removed at high regeneration temperature. Even though less coke deposition was observed at regeneration temperature above 400°C, the catalytic performance was decreased. This is due to the high amount of PtSn alloys was broken at high regeneration temperature. Moreover, catalyst will lose it structure especially at 500°C. At this condition, the TPR profile shifts to higher temperature and H_2 consumption decreases strongly. It may be attributed to Sn species migrated to the support. From the catalytic activity measurement, Regeneration at 400°C seems to be suitable temperature for the regeneration deactivated 1Pt1Sn/COM catalysts because high amount of PtSn alloys and low residual coke deposits were observed.

(II) X-Ray Photoelectron Spectroscopy (XPS)

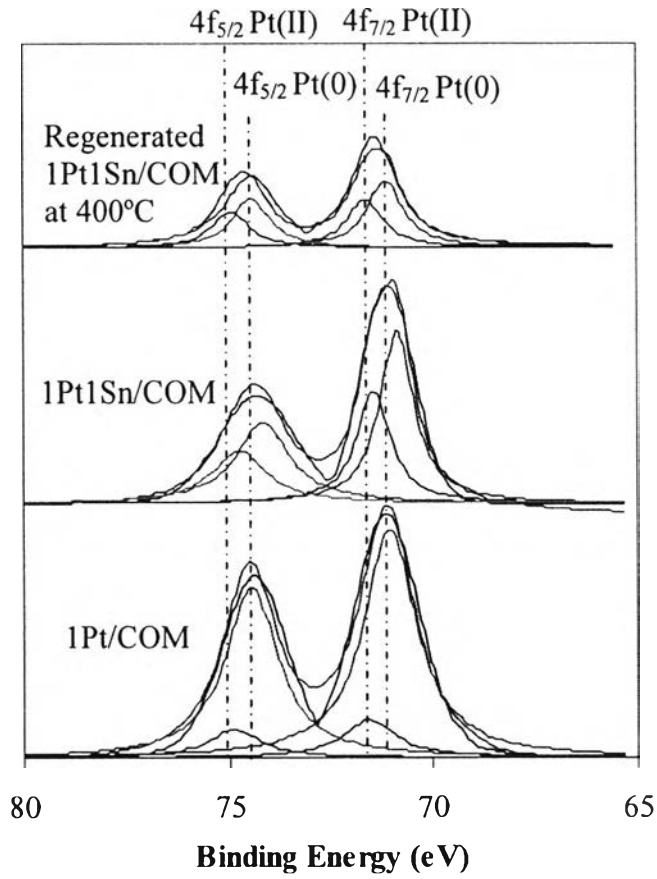

Figure 4.15 Pt4f XPS spectra of 1Pt/COM, 1Pt1Sn/COM and regenerated 1Pt1Sn/COM catalyst in air at 400°C after hydrogen treatment for 1 h at 500°C (reduced).

The oxidation states of 1Pt/COM, 1Pt1Sn/COM and regenerated 1Pt1Sn/COM catalyst in air at 400°C after reduction with hydrogen for 1 h at 500°C were investigated by XPS. Figure 4.15 reports the Pt 4f region of 1Pt/COM, 1Pt1Sn/COM and regenerated 1Pt1Sn/COM catalyst in air at 400°C. The relative intensities of different species from the curve-fitted XP spectra and their binding energy (B.E.) are reported in Table 4.6.

Table 4.6 Binding energies and relative intensities of different species from curve-fitted XPS spectra of various catalysts

Sample	Species	Binding Energy (eV)		Relative Peak Area (%)
1Pt/COM		Pt $4f_{7/2}$	Pt $4f_{5/2}$	
	Pt(0)	71.05	74.45	85.82
	Pt(II)	71.57	74.87	14.18
1Pt1Sn/COM		Pt $4f_{7/2}$	Pt $4f_{5/2}$	
	Pt(0)	70.87	74.17	60.44
	Pt(II)	71.44	74.74	39.56
Regenerated 1Pt1Sn/COM at 400°C		Pt $4f_{7/2}$	Pt $4f_{5/2}$	
	Pt(0)	71.13	74.43	57.67
	Pt(II)	71.63	74.93	42.33

The Pt4f photoelectron line mainly consists of two doublets of increasing binding energies (B.E.), assigned to Pt metal and PtO. The presence of metallic Pt(0) of 1Pt/COM, characterized by the $4f_{7/2}$ and $4f_{5/2}$ peak doublet with the B.E at 71.05 and 74.45 eV, respectively (Hoang *et al.*, 2007). The presence of the above reported oxidized platinum species is quite evident at higher B.E. (Neri *et al.*, 2007), i.e. PtO at about 71.57 and 74.87. After addition of Sn, when PtSn alloys were formed, an electron transfer from Sn to Pt can occur. Consequently, $Pt4f_{7/2}$ components which gain electronic density from Sn are shift to lower B.E. as shown in Figure 4.15 and Table 4.6. Most recently, it was found that observed a similar shift towards lower B.E. for the $Pt4f_{7/2}$ signal of Pt-Sn/SiO_2 catalysts prepared by surface organometallic reactions versus Pt/SiO_2. This effect was attributed to an electron transfer from Pt4f level to the Pt–Sn bond. Moreover, the interesting change was observed on the regenerated 1Pt1Sn/COM at 400°C in air. $Pt4f_{7/2}$ of Pt(0) is shifted to the higher B.E. compared to the bimetallic 1Pt1Sn/COM, indicating the loss of PtSn

alloys. In good agreement with TPR, XPS shows the breakage of Pt-Sn alloys after regeneration.

(III) Temperature Programmed Oxidation (TPO)

The spent and regenerated catalysts were also characterized by TPO to determine the amount of carbon deposits on the catalysts in term of percent weight of carbon.

Table 4.7 shows amount of carbon deposits in the spent and regenerated Pt-Sn/COM catalysts at different regeneration temperatures.

Table 4.7 TPO analysis of spent and regenerated 1Pt1Sn/COM catalysts at different regeneration temperatures

Temperature of regeneration (°C)	Time of regeneration (min)	Air flow rate (ml/min)	%C (wt.%)
300	30	20	1.27
350			0.90
400			0.87
450			0.49
500			0.22
Spent 1Pt1Sn/COM (after 550 min on stream)			2.58

It was observed that the amount of coke burned corresponded to the temperature of regeneration that the higher regeneration temperature, the higher percent carbon removal. In other words, the lower regeneration temperature, the higher coke formation in the regenerated catalysts as shown in Table 4.7. According to the TPR profiles (Figure 4.14), it can be confirmed that a desorption peak appears at high temperature (above 400°C) when without regeneration and regeneration at low temperature (300°C and 350°C) was caused by high coke deposition leading to pore blocking of L-zeolite. This explanation was corresponded to high EB/OX ratio obtained at low regeneration temperature (300°C). Therefore, regenera-

tion temperature should be high enough in order to burn coke; on the other hand, it should not be too high to avoid the catalyst lost its structure.

4.4.2 Effect of Regeneration Time

In this part, catalytic activity measurement and catalyst characterization were discussed.

4.4.2.1 Catalytic Activity Measurement

The reaction-regeneration cycles were performed under a constant regeneration temperature and air flow rate at various regeneration times from 15 min to 120 min. The comparison among the different regeneration times was investigated in term of catalytic activity after 370 min on stream after reaction-regeneration cycles as demonstrated the previous effect.

Figure 4.16 to Figure 4.19 show the *n*-octane conversion, C8-aromatics selectivity, total aromatics selectivity and EB/OX ratio after 370 min on stream of catalyst regenerated with air at various regeneration times (15-120 min), respectively. The regeneration in the range of 15-60 min is slightly different but the regeneration for 15 min a little higher. When the regeneration time is longer than 60 min, the *n*-octane conversion will decrease.

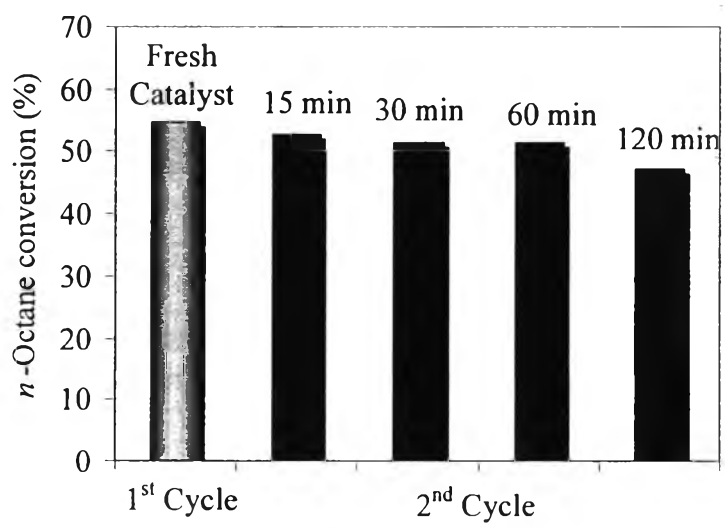

Figure 4.16 The *n*-octane conversion after 370 min on stream of regenerated catalysts at various regeneration times (15-120 min).

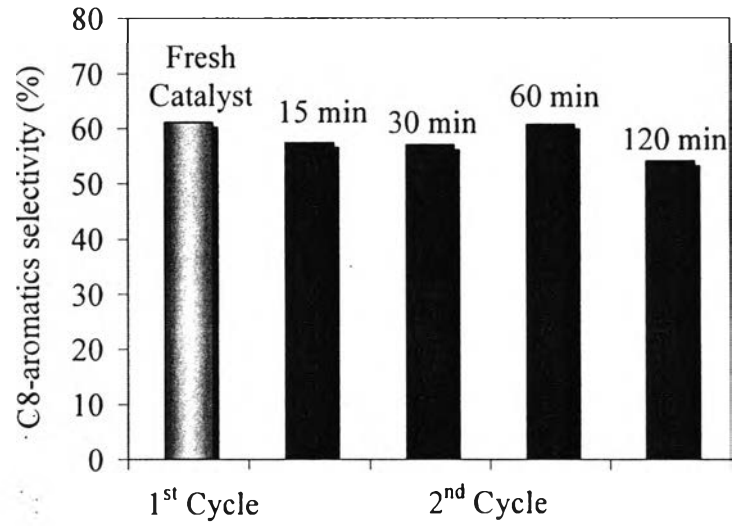

Figure 4.17 The C8-aromatics selectivity after 370 min on stream of regenerated catalysts at various regeneration times (15-120 min).

Although the regeneration time of 15 min exhibits a little higher *n*-octane conversion compared to the other, the regeneration for 60 min resulted in the highest C8 aromatics selectivity, as shown in Figure 4.17, which is one of the main criteria to evaluate the optimal conditions in this work.

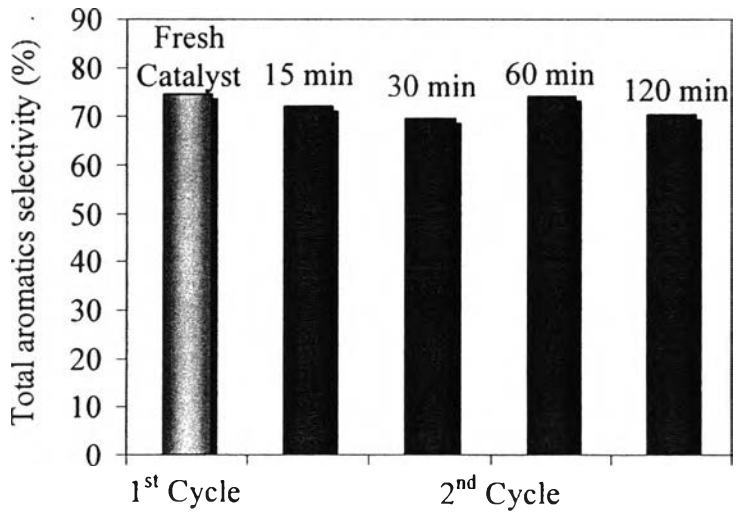

Figure 4.18 The total aromatics selectivity after 370 min on stream of regenerated catalysts at various regeneration times (15-120 min).

According to Figure 4.18, the variation of aromatics selectivity was not significantly influenced by the regeneration time. The regeneration for 60 min obtained the variation of aromatics selectivity which is closely to the fresh catalyst.

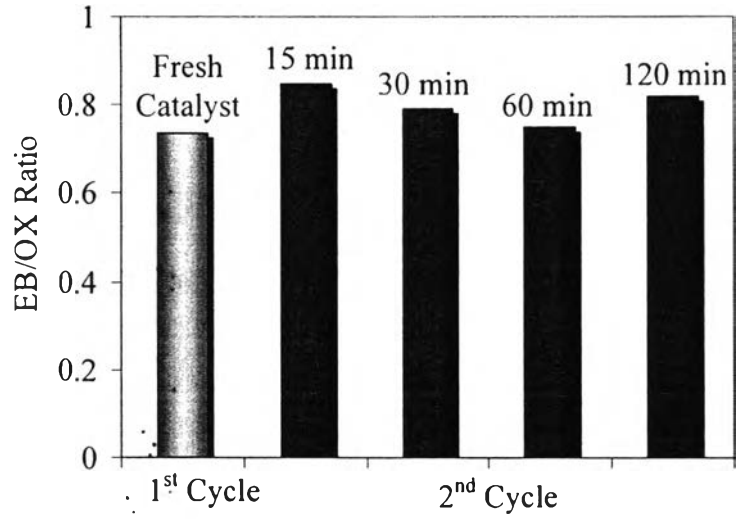

Figure 4.19 The EB/OX ratio after 370 min on stream of regenerated catalysts at various regeneration times (15-120 min).

The regeneration time for 60 min obtained lowest EB/OX ratios. When the time of regeneration is too long, the EB/OX ratios will be higher as illustrated in Figure 4.19.

4.4.2.2 Characterization of Catalysts

Fresh, spent and regenerated catalysts were characterized by means of TPR and TPO.

(I) Temperature Programmed Reduction (TPR)

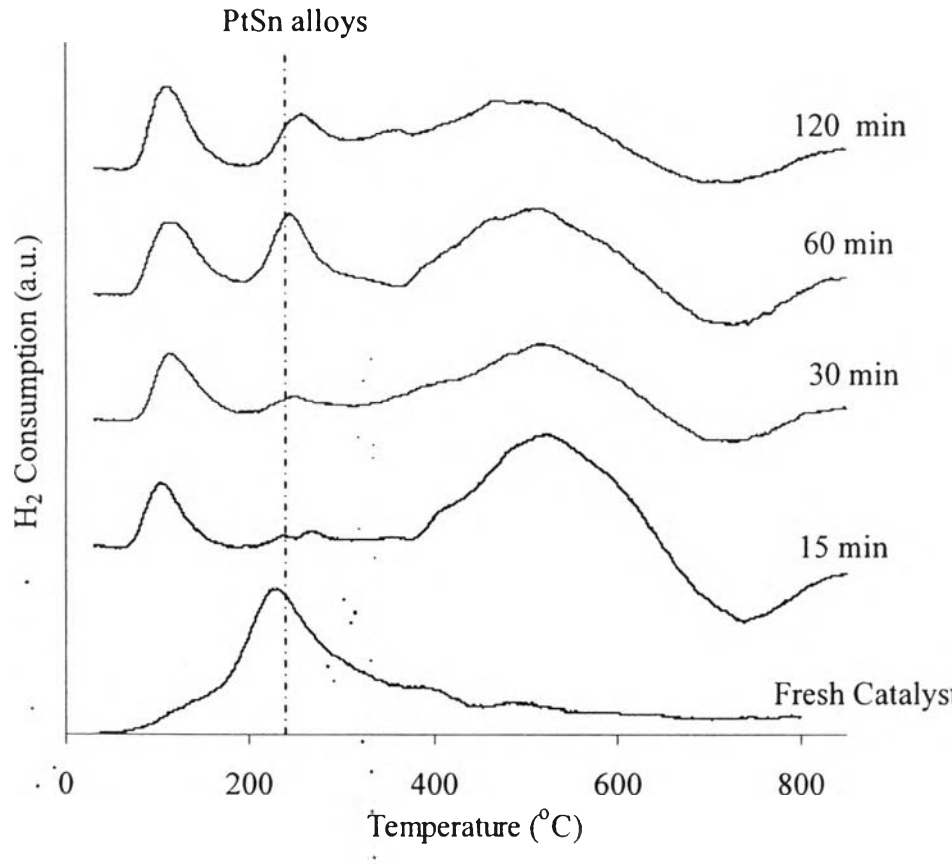

Figure 4.20 TPR profiles of regenerated catalysts at various regeneration times (15-120 min).

The TPR profiles of the regenerated catalyst at various times display the result that corresponds to the previous section (Section 4.4.1.1). The second area peak (PtSn alloys) shifts slightly from 240°C to 250°C. Interestingly, when the regeneration time increased, the second area peak (PtSn alloys) showed a large increase in the intensity and a desorption peak at high temperature showed a small decrease in the intensity because coke deposits decrease markedly. It means that short time is not sufficient to restore completely the structural properties on the sample. Regeneration at 400°C for 60 min exhibits high amount of PtSn alloys as shown in Figure 4.20.

(II) Temperature Programmed Oxidation (TPO)

From Table 4.8 shows that there was no significant change in carbon remained in the regenerated catalysts when regeneration time was increased from 30 min to 120 min. When regeneration time prolong from 15 min to 30 min, amount of coke formation was decreased sharply and then slightly decreased at regeneration time above 30 min. This was in good agreement with the result obtained from characterization by TPR. It was concluded that the suitable regeneration temperature should be long enough in order to burn high amount of coke.

Table 4.8 TPO analysis of spent and regenerated 1Pt1Sn/COM catalysts at different regeneration times

Temperature of regeneration (°C)	Time of regeneration (min)	Air flow rate (ml/min)	%C (wt.%)
400	15	20	1.23
	30		0.32
	60		0.29
	120		0.28
Spent 1Pt1Sn/COM (after 550 min on stream)			2.58

4.4.3 Effect of Regeneration Air Flow Rate

In this part, catalytic activity measurement and characterization of catalysts will be discussed.

4.4.3.1 Catalytic Activity Measurement

The reaction-regeneration cycles were performed under a constant regeneration temperature and regeneration time operated under 10, 20, 40 ml/min in each reaction-regeneration cycle.

Figure 4.21 to Figure 4.24 show the *n*-octane conversion, C8-aromatics selectivity, total aromatics selectivity and EB/OX ratio after 370 min on

stream of catalyst regenerated with air at various regeneration air (as coke oxidant mixture) flow rates (10-40 ml/min), respectively.

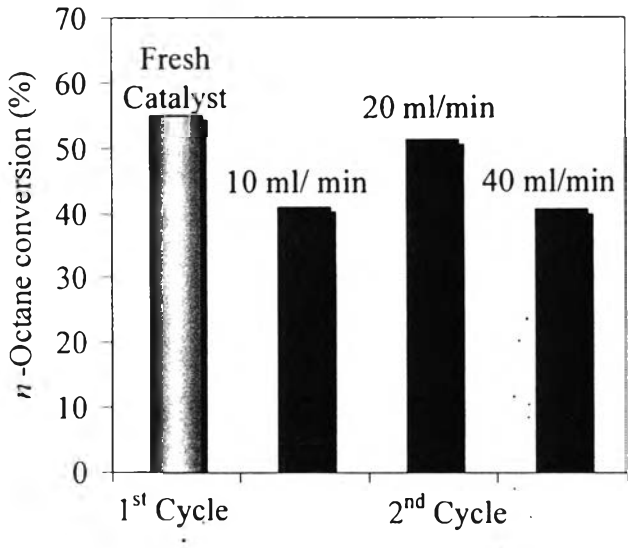

Figure 4.21 The *n*-octane conversion after 370 min on stream of regenerated catalysts at various regeneration air flow rates (10-40 ml/min).

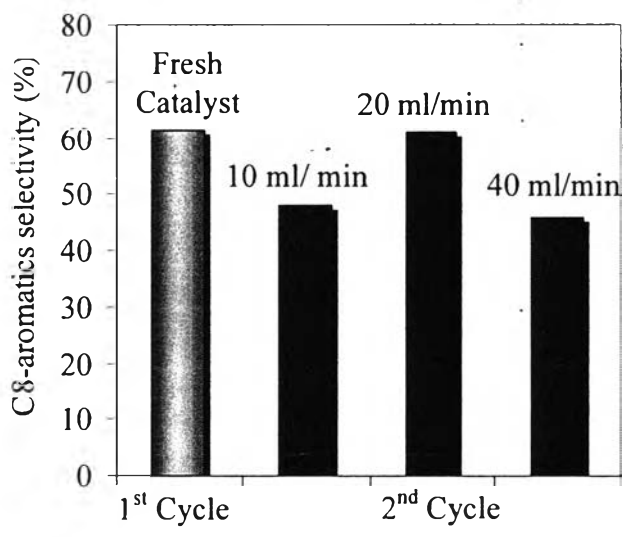

Figure 4.22 The C8-aromatics selectivity after 370 min on stream of regenerated catalysts at various regeneration air flow rates (10-40 ml/min).

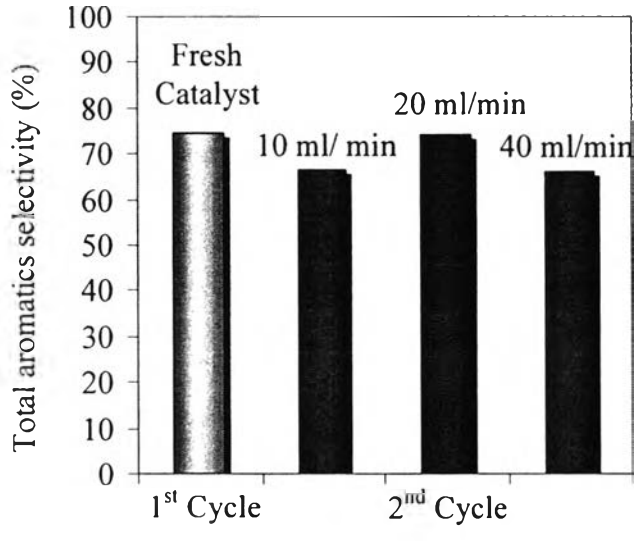

Figure 4.23 The total aromatics selectivity after 370 min on stream of regenerated catalysts at various regeneration air flow rates (10-40 ml/min).

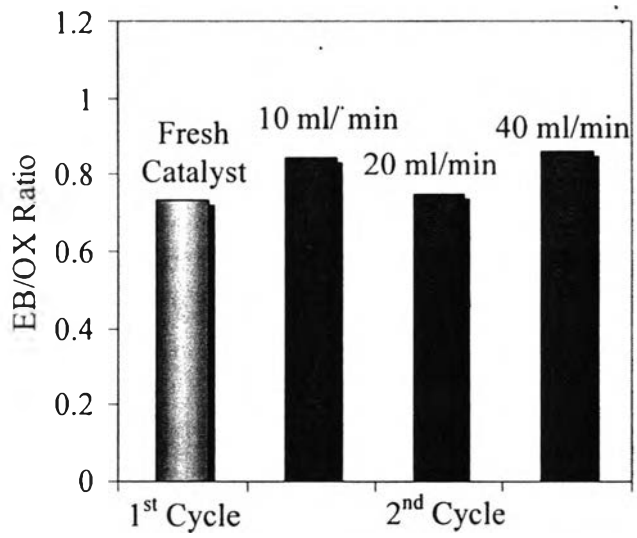

Figure 4.24 The EB/OX ratio after 370 min on stream of regenerated catalysts at various regeneration air flow rates (10-40 ml/min).

According to Figure 4.21 and Figure 4.22, the suitable air flow rate for regeneration of spent 1Pt1Sn/COM is 20 ml/min. Since less air flow rate is not enough to remove the deposited coke. In addition, excess air flow rate is not good for catalyst regeneration. The *n*-octane conversion at these air flow rate performs highest variation conversion that can be regained closely to the original of the fresh

1Pt1Sn/COM. Regeneration in air at 20 ml/min resulted in exactly the highest C8-aromatics selectivity among the other flow rate and exhibited the higher total aromatics selectivity than other flow rate as observed in term of catalytic activity as shown in Figure 4.23. Finally, Air flow rate of 20 ml/min is enough to remove coke deposits covering the PtSn alloys; consequently, EB/OX ratio is lower closely to the original catalyst compared to other air flow rate as shown in Figure 4.24.

4.4.3.2 Characterization of Catalysts

Fresh, spent and regenerated catalysts were characterized by means of TPR and TPO.

(I) Temperature Programmed Reduction (TPR)

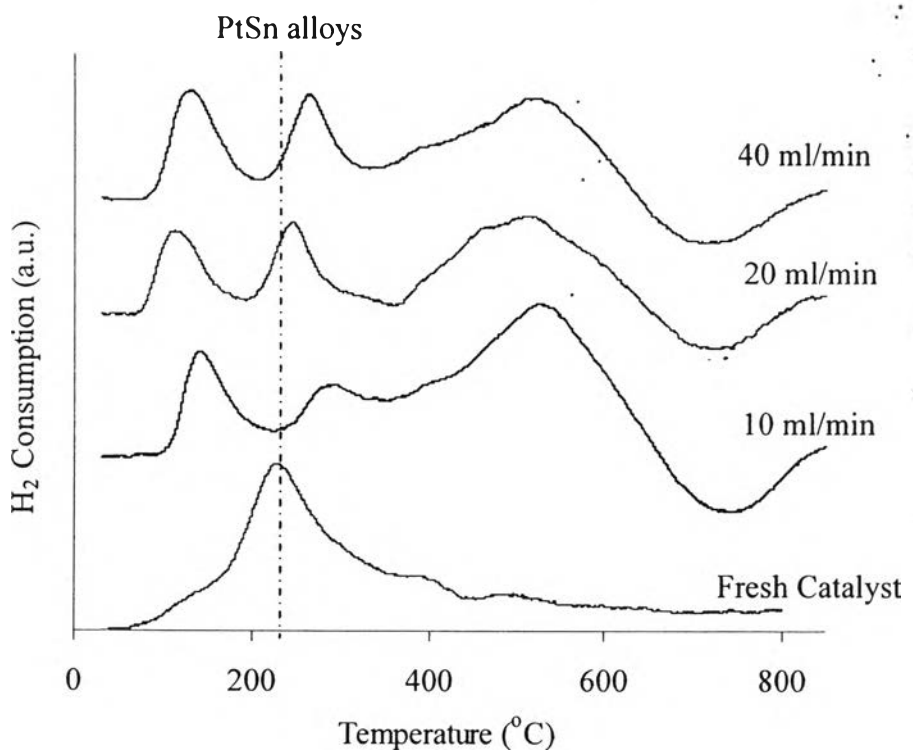

Figure 4.25 TPR profiles of regenerated catalysts at various regeneration air flow rates (10-40 ml/min).

Figure 4.25 shows TPR profiles of fresh and regenerated Pt-Sn/COM catalysts in air flow rate of 10, 20 and 40 ml/min. The TPR profiles correspond to

two previous sections (Section 4.4.1.1 and 4.4.1.2). It was investigated that a shift of second peak in TPR profile to higher temperature was significantly observed in the all regenerated catalysts when compare to the TPR profile of the fresh catalyst. The "standard" (20 ml/min) air flow rate was enough for restoring the original metallic state at 400°C as shown in Figure 4.25. For slow air flow rate (10 ml/min), the second peak appeared at 292°C significantly changed position compared with the fresh catalyst which appeared at 233°C and the second peak was not shown sharply as the others. It might be due to high amount of coke deposits on the catalyst because the air flow rate is not high enough to remove the carbon content. On the other hand, for high air flow rate (40 ml/min) the profile seem to be very close to that of the standard air flow rate. An adsorption peak still appears at high temperature (400°C).

(II) Temperature Programmed Oxidation (TPO)

The result shows that there was no significant change in carbon remained in the regenerated catalysts at different air flow rate as shown in Table 4.9. It was found that regeneration in air at 10 ml/min gives remarkably the high coke formation. These results were good agreement with the results obtained from the TPR as demonstrated in Figure 4.25.

Table 4.9 TPO analysis of spent and regenerated 1Pt1Sn/COM catalysts at different regeneration air flow rates

Temperature of regeneration (°C)	Time of regeneration (min)	Air flow rate (ml/min)	%C (wt.%)
400	60	10	0.42
		20	0.31
		40	0.36
Spent 1Pt1Sn/COM (after 550 min on stream)			2.58

In conclusion, regeneration via coke oxidation in air at 400°C, 120 min, air flow rate = 20 ml/min was selected to be the regeneration condition provided 91.34% of coke removed from spent Pt-Sn/COM catalysts.